



# Lithosphere of South American intracratonic basins: Electromagnetic and potential field data reveal cratons, terranes, and sutures

Gabriel N. Dragone<sup>a,\*</sup>, Mauricio S. Bologna<sup>a</sup>, Naomi Ussami<sup>a</sup>, Mario E. Giménez<sup>b,c</sup>, Orlando Alvarez<sup>b,c</sup>, Federico G. Lince Klinger<sup>b,c</sup>, Sebastián Correa-Otto<sup>b,c</sup>

<sup>a</sup> Universidade de São Paulo, Instituto de Astronomia, Geofísica e Ciências Atmosféricas, Departamento de Geofísica, São Paulo, Brazil

<sup>b</sup> Instituto Geofísico Sismológico Volponi (IGSV), Universidad Nacional de San Juan, Facultad de Ciencias Exactas, Físicas y Naturales, San Juan, Argentina

<sup>c</sup> Consejo Nacional de Investigaciones Científicas y Técnicas (CONICET), Argentina

## ARTICLE INFO

### Keywords:

Magnetotellurics  
Density  
Cratons  
Sutures  
Rio Tebicuary  
Paraná

## ABSTRACT

A magnetotelluric survey comprising 18 broadband stations disposed along a 450 km-long profile was carried out at the transition between the Chaco-Paraná (CPB) and the Paraná (PB) intracratonic basins in northeastern Argentina. Three-dimensional inversions of the responses show that the CPB and southern PB lithospheres are resistive ( $\sim 10^3 \Omega \text{ m}$ ) down to 120 km, but with distinct crustal and upper mantle electrical properties. Also, Bouguer gravity and density anomalies are positive at CPB, whereas they are negative at PB. We associate the CPB lithosphere with the Paleoproterozoic Rio Tebicuary craton and the southern PB lithosphere with an ancient and buried piece of craton, the Southern Paraná craton. Geochemical data of mantle xenoliths from the Cenozoic alkaline/carbonatitic province within the Rio Tebicuary craton suggest a subcontinental lithospheric mantle affected by metasomatic processes, which explains its lower resistivity (reaching values as low as  $300 \Omega \text{ m}$ ) and higher density ( $\#Mg = 0.87$ ). In contrast, the Southern Paraná craton is more resistive ( $>10^3 \Omega \text{ m}$ ) and less dense, suggesting a de-hydrated, depleted, and thicker craton. These cratons are separated by a crustal conductor (15 to 20 km depth;  $1\text{--}10 \Omega \text{ m}$ ) that we interpret as a southward continuation of a linear anomaly (Paraná Axial Anomaly) defined in former induction studies within the PB in Brazil. Hence, we redefined the trace of this conductive lineament: instead of bending towards the Torres Syncline, it continues inside the CPB. We propose the lineament to be an Early Neoproterozoic suture zone that controlled the location of maximum subsidence in the intracratonic basins during the Paleozoic. In the Early Cretaceous, the Paraná Axial Anomaly was the site of maximum extrusion and deposition of Serra Geral basalts. This anomaly separates compositionally distinct cratonic lithospheres along its path. Melting of this heterogeneous and enriched mantle created the Paraná igneous province.

## 1. Introduction

The South American protocontinent was formed through the assemblage of different tectonic units by means of processes involving collisions, subductions, and shearing from the Proterozoic until the Eopaleozoic (de Almeida et al., 2000; Ramos, 1988). However, its geologic framework is nowadays widely concealed under intracratonic sedimentary basins. The geodynamic processes that take place during the evolution of intracratonic basins are the least known from all types of sedimentary basins (Allen and Allen, 2013). Long-term subsidence time span ( $>200 \text{ My}$ ) and large areas of surface depression suggest an interaction between the lithosphere and the sublithospheric mantle

during the evolution of intracratonic basins.

In the present study (Fig. 1), we investigate two geophysical properties of the lithosphere, electrical resistivity and density, under the Chaco-Paraná and Paraná intracratonic basins as a continuation of recent efforts to combine geophysical techniques to study the lithosphere of the South American plate (e.g. Bologna et al., 2019; Chaves et al., 2016). Ultimately, we aim to understand the dynamic processes responsible for the subsidence of large areas on the Earth surface, and why some of these basins were also affected by extensive volcanism turning into large igneous provinces (LIP), such as the Paraná-Etendeka.

The intracratonic Chaco-Paraná and Paraná basins (Fig. 2a) developed in southeastern South America. Due to their proximity and

\* Corresponding author.

E-mail address: [gabriel.dragone@usp.br](mailto:gabriel.dragone@usp.br) (G.N. Dragone).

<https://doi.org/10.1016/j.tecto.2021.228884>

Received 20 September 2020; Received in revised form 5 April 2021; Accepted 16 April 2021

Available online 23 April 2021

0040-1951/© 2021 Elsevier B.V. All rights reserved.

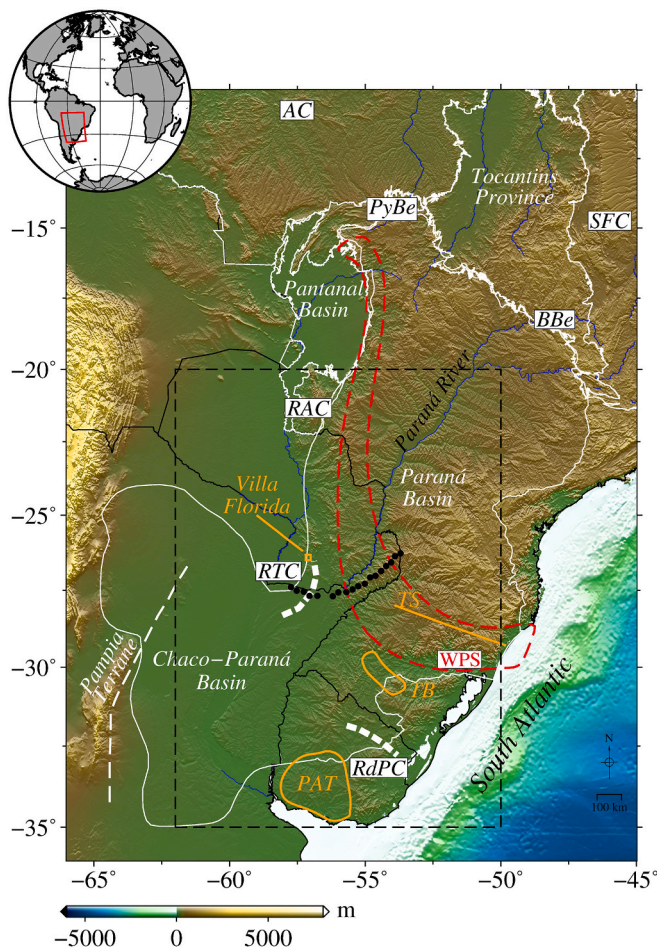


**Fig. 1.** Topographic map (ETOPO1, [Amante and Eakins, 2009](#)) with basins and tectonic provinces outlined in solid white. Black dots are the MT stations used in this work. Dashed white lines are the partial limits of terranes and cratons based on geophysical data: Pampia terrane (cf. [Favetto et al., 2015](#)); RdPC – Rio de la Plata craton ([Bologna et al., 2019](#)); RTC – Rio Tebicuary craton ([Dragone et al., 2017](#), and this study). Orange contours are superficial geological units: PAT – Piedra Alta terrane; TB – Taquembó block; TS – Torres syncline. The Paleoproterozoic Villa Florida Metamorphic Suite is drawn after [Leite et al. \(2018\)](#). The dashed red line is the WPS – Western Paraná Suture/Shear zone ([Dragone et al., 2017](#)). Other abbreviated units: AC – Amazon craton; BBe – Brasília Belt; PyBe – Paraguay Belt; RAC – Rio Apa craton; SFC – São Francisco craton. The dashed black square is the region shown in [Fig. 2](#). (For interpretation of the references to colour in this figure legend, the reader is referred to the web version of this article.)

partially coincident stratigraphic columns, they have been considered as a single depositional system initiated in the Neoproterozoic and were set apart from the Mesozoic on ([Milani and Zalán, 1999](#); [Pezzi and Mozetic, 1989](#)). The trigger of this independent evolution seems to be associated with the Serra Geral flood magmatism in the Early Cretaceous ( $134.7 \pm 1$  Ma; [Renne et al., 1992](#); [Thiede and Vasconcelos, 2010](#)) that generated the Paraná-Etendeka LIP. Part of the magmatic material was retained in the lower crust ([Mariani et al., 2013](#)), causing a regional uplift due to isostatic compensation. With a total thickness of sedimentary rocks and basalts reaching up to 7 km in the Paraná basin and 4 km in the Chaco-Paraná, most of the tectonic fabric and age of their basements remain poorly known, with information provided by scarce wells and geophysical data.

Using the most comprehensive gravity model to date for the South American platform, the SAGM04 ([de Sá, 2004](#), see [Fig. 2b](#)), [Dragone et al. \(2017\)](#) delimited the Western Paraná Suture/shear zone (WPS). The WPS follows a gravity gradient coincident with granites of

Neoproterozoic age that separates the Paraná basin lithosphere, where negative Bouguer anomalies prevail ( $\sim -70$  mGal), from surrounding units such as the Rio Apa, Rio Tebicuary and Rio de la Plata cratons to the west and south, all with positive Bouguer anomalies ( $\sim 10$  mGal). The WPS mostly reflects crustal thickness variations, since the Chaco-Paraná basin crust is thinner (35–40 km) than the Paraná basin crust (40–45 km; cf. [Rivadeneira-Vera et al., 2019](#)), but it also accounts for differences in lithosphere properties such as electrical resistivity and seismic velocity (cf. [Dragone et al., 2017](#)).

To study in greater detail the transition in physical properties across the WPS, we conducted a broadband (0.001–3200 s) magnetotelluric (MT) survey crossing this discontinuity. Our MT profile starts at the gravity high located in the Chaco-Paraná basin and continues towards a gravity low in the southwestern Paraná basin ([Fig. 2b](#)).

The MT method uses the Earth's naturally occurring electric and magnetic fields as a source for imaging the electrical resistivity distribution of the subsurface. It ranges from depths as shallow as dozens of meters to depths as deep as hundreds of kilometers. The MT method has been used with success to map tectonic features, such as fossil suture zones, relics of subductions, and delimiting terrane boundaries in cratonic areas, as in the Kaapval and Congo cratons ([Evans et al., 2011](#); [Khoza et al., 2013](#)). The new MT data provided a three-dimensional geoelectrical model in the transition between the Chaco-Paraná and Paraná basins in northeastern Argentina.

Integrating gravity and magnetic data and the results of the present MT study with published geoelectrical sections across suture zones around and within the Chaco-Paraná and Paraná basins, we demonstrate that their lithospheric structures are distinct. The Paraná basin is surrounded by several suture zones and its lithosphere is composed of an assemblage of cratonic blocks and terranes. We also demonstrate that a suture zone associated with a conductive lineament named Paraná Axial Anomaly (PAA, [Maurya et al., 2018](#)) continues into Argentina. By reconstructing SW Gondwana assemblage, we try to date PAA considering the Neoproterozoic-Cambrian age of the WPS. At last, we present a brief discussion on the distinction between Chaco-Paraná and Paraná lithospheres with emphasis on the latter turning into a LIP in the Early Cretaceous.

## 2. MT data processing and analysis

### 2.1. Field data

Broadband MT data were acquired at 18 stations using a five-component system (Metronix ADU07e). The stations are evenly distributed, with an average spacing of 25 km, along a 450 km-long profile. The two orthogonal components of the electrical field ( $E_x$  and  $E_y$ ) were measured with lead-lead chloride electrodes (Pb-PbCl<sub>2</sub>) disposed in two dipoles of about 100 m, with the x-component aligned to the geomagnetic north. The three mutually orthogonal components of the magnetic field ( $H_x$ ,  $H_y$ , and  $H_z$ ) were measured with highly sensitive induction coils. The record duration at each station varied from 32 to 48 h, covering periods ranging from 0.001 to 3200 s.

The four elements of the impedance tensor (MT transfer functions) and the two elements of the vertical magnetic transfer function (also known as tipper) were estimated with a robust multiple station code ([Egbert, 1997](#)). The geomagnetic declination (recording azimuth) was stored in the final processed files for later reference during data analysis. All stations yielded high-quality data, except for the dead band (1–10 s) at station 09. Additionally, data from station 03 were partially lost due to a malfunction in the  $H_y$  magnetometer cable. The period interval resulting from the processed time series allows the MT fields to sample internal structures within the basins down to upper mantle depths.

[Fig. 3](#) shows the apparent resistivity and phase curves for the XY and YX components at two representative stations (02 and 17). The curves of all stations can be found in the Supplementary Material ([Fig. S1](#)). The MT curves are coherent with the superficial geology and the overall

structure and composition of the basin layers as predicted by geophysical well logs. Station 02 is in the Chaco-Paraná basin, where Quaternary deposits of Andean provenance outcrop, whereas station 17 is in the Paraná basin, where basalts of the Serra Geral Formation cover the surface. This difference in superficial lithology is manifested in the apparent resistivities at the shortest periods, which are lower at station 02 ( $\sim 30 \Omega \text{ m}$ ) than at station 17 ( $\sim 10^2 \Omega \text{ m}$ ). The minimum between 0,1 and 1 s in both stations' resistivity curves is related to pre-volcanic sedimentary rocks, and the subsequent upward inflection is due to the contact between the sedimentary layer and the electrical basement of the basins. It occurs earlier at station 02 ( $\sim 0.3 \text{ s}$ ) than at station 17 (10 s), indicating that the Chaco-Paraná basin is thinner than the Paraná basin at the location of these stations.

## 2.2. Induction arrows

The tipper, which relates the vertical component of the magnetic field to the horizontal ones, is graphically represented by induction arrows. Fig. 4 shows the real induction arrows for periods of 26, 204, and 1170 s in the Parkinson convention, in which arrows point towards conductive structures.

At short periods induced electric currents flow dominantly in the conducting sequences of the Chaco-Paraná and Paraná basins, so the arrows amplitudes are very small in all MT stations. Significant amplitudes begin to be observed only at periods longer than 26 s.

In the western portion of the study area, between stations 01 and 07, the induction arrows at 26 s show relatively large amplitudes, probably related to structures in the geoelectric basement. In particular we observe a reversion of the induction arrows between stations 04 and 06

that persists until 204 s. This reversion indicates that a conductive structure perpendicularly crosses the MT profile between these stations.

At 204 s, between stations 07 and 18, the arrows point systematically towards the NW, indicating the existence of a conductive feature parallel to the MT profile. This behavior persists at longer periods, suggesting that the off-profile structure is a regional anomaly. At 1170 s, the complete reversion is no longer observed. Although the induction arrow at station 06 still points to the west, the arrow at station 04 now points southwards. This change in direction may indicate that the off-profile structure extends to the south, but this is uncertain due to the lack of vertical field data in this part of the profile.

## 2.3. Dimensionality analysis

Data dimensionality was assessed using the phase tensor proposed by Caldwell et al. (2004) and Bibby et al. (2005). According to the authors, the phase tensor is insensitive to distortions caused by small-scale heterogeneities. Hence the method can provide reliable information about the subsurface dimensionality. The phase tensor ellipticity ( $\lambda$ ) and skew angle ( $\beta$ ) are coordinate invariants and are related with the impedance tensor dimensionality at a single period and station. In a 1-D case, both  $\lambda$  and  $|\beta|$  should be close to zero or less than their respective threshold values, usually and respectively considered 0.1 and  $3^\circ$  in the literature ( $\lambda < 0.1$ ;  $|\beta| < 3^\circ$ ). In a 2-D case,  $\lambda$  is higher than its threshold value, while  $\beta$  is still lower than the threshold value ( $\lambda > 0.1$ ;  $|\beta| < 3^\circ$ ). In a 3-D case, both invariants are higher than their threshold values ( $\lambda > 0.1$ ;  $|\beta| > 3^\circ$ ).

Phase tensor elements and their coefficients were calculated at each station (Fig. 5). Since the data dimensionality depends on threshold

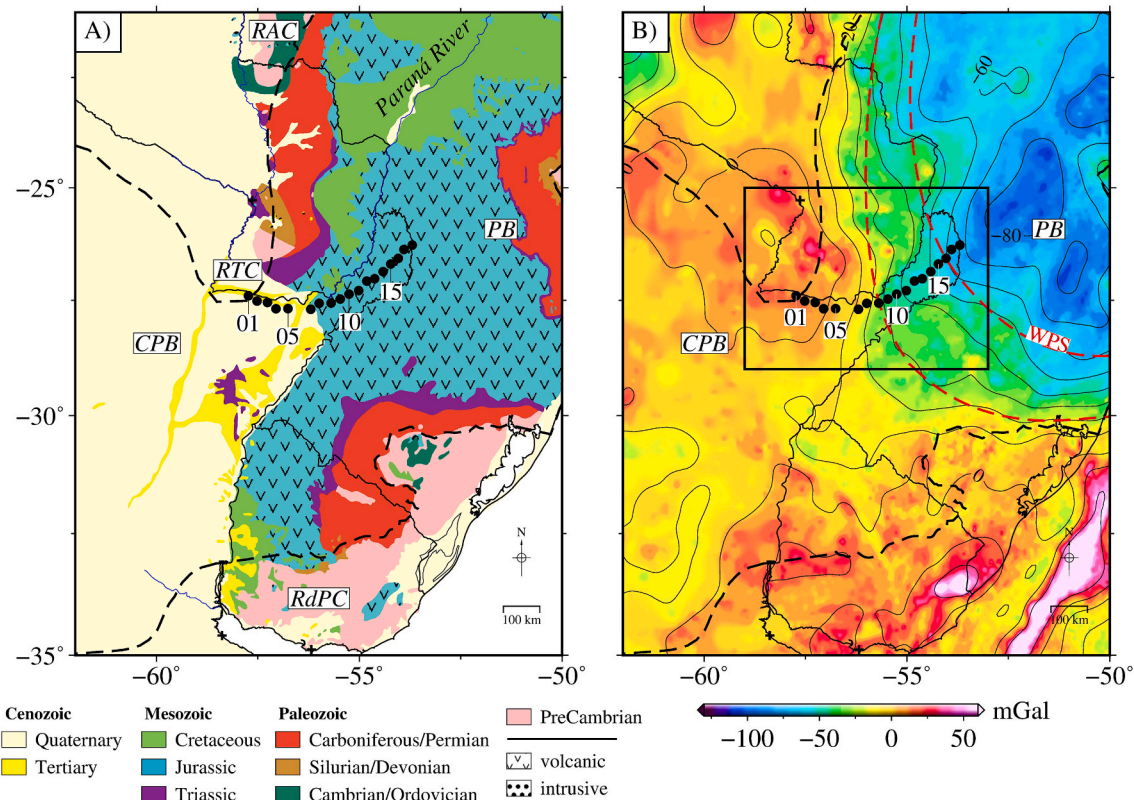
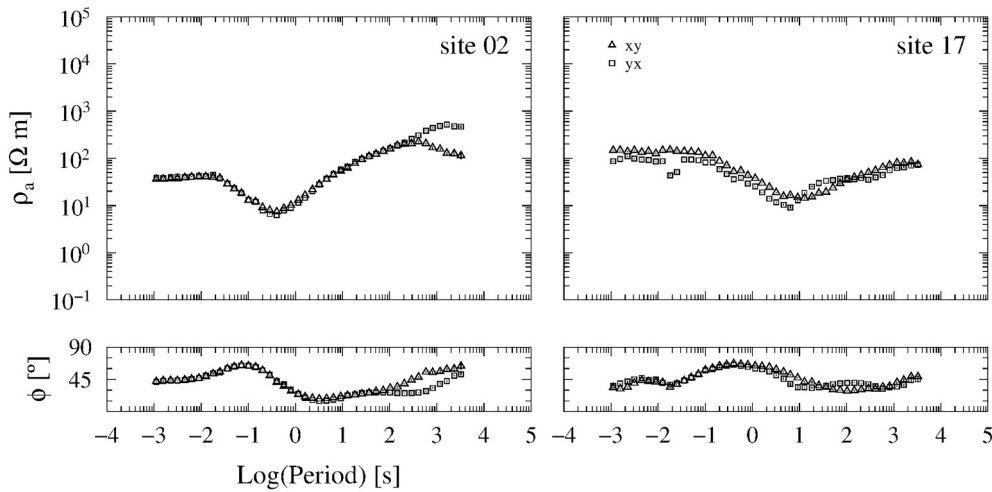
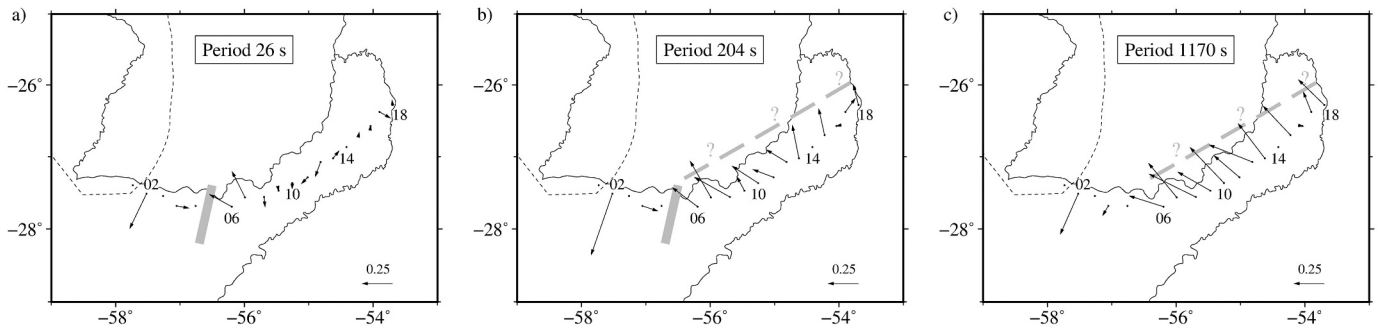


Fig. 2. (a) Geological map adapted from the USGS (Schenk et al., 1999). Black dots are the MT stations. Dashed black lines are the Chaco-Paraná and Paraná basins limits. See legend for details on geology. (b) Gravity map from the SAGM04 model (de Sá, 2004), composed of Bouguer anomalies on the continent and free-air anomalies on the ocean. Colour scale values are at the geoid. Black contours are gravity anomalies upward continued to 30 km height at 10 mGal intervals. The dashed red line is the WPS (Dragone et al., 2017). Abbreviated units: CPB – Chaco-Paraná basin; RAC – Rio Apa craton; RdPC – Rio de la Plata craton; RTC – Rio Tobicuary craton; PB – Paraná basin; WPS – Western Paraná Suture/Shear zone. (For interpretation of the references to colour in this figure legend, the reader is referred to the web version of this article.)



**Fig. 3.** Measured apparent resistivities and phases for two representatives MT soundings, stations 02 and 17, obtained in a coordinate system with the x-axis aligned with the geomagnetic north. Triangles and squares represent the MT responses from the electric dipoles oriented N13°W and N77°E for station 02, and N16°W and N74°E for station 17, respectively.



**Fig. 4.** Real induction arrows for periods (a) 26 s, (b) 204 s, and (c) 1170 s. The solid gray bar indicates the location of a reversion. The dashed gray line is perpendicular to all arrows in the eastern part of the profile.

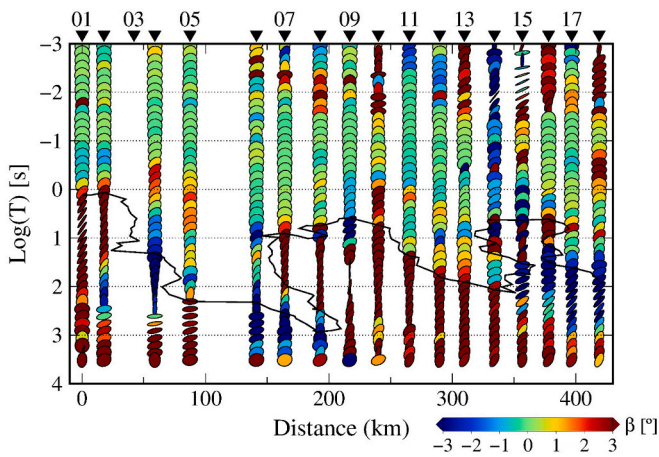


**Fig. 5.** Phase tensor ellipsis with major axes normalized by the minor axes. The colour filling represents the skew angle ( $\beta$ ). The black contour is a rough  $\pm 3^\circ$  limit, indicating the 3-D domain.

values, errors play a major role and were propagated from the impedance tensor to the phase tensor using the delta method as described in Patro et al. (2013, see their Appendix). We provide a brief discussion on errors in the Supplementary Material (Fig. S2).

Overall, most data for periods shorter than 1 to 10 s are within the 1-

D dimensionality threshold, with  $\lambda$  close to zero and  $|\beta| < 3^\circ$ . Induction arrows at these short periods in the eastern part of the profile also present small amplitude, as observed in Fig. 4(a), indicating a 1-D environment. This is a consequence of the fact that the phase tensor and tipper responses at these periods are controlled by the sedimentary layers of the basins. The western part of the profile is already affected by the electrical basement at 26 s, however the induction arrows present small amplitude below 10 s (not shown), in accordance to the phase tensor.

For longer periods ( $>10$  s), stations 05 and 06 are within the 2-D threshold ( $|\beta| < 3^\circ$ ) until 200 s. The induction arrows at this portion of the profile also points to a 2-D scenario, with the occurrence of a reversion in the arrows indicating the possibility of a conductive structure perpendicularly crossing the MT profile.

Except for stations 05 and 06, most data for periods above 10 s are 3-D since their beta-values are higher than the stipulated limits ( $|\beta| > 3^\circ$ ). This could indicate the presence of an off-profile structure along these stations. Once again, the induction arrows are in accordance with the phase tensor observations, since the arrows consistently point to the NW at the eastern part of the profile suggesting the occurrence of a parallel conductive structure there (Fig. 4b and c). Since this study focuses on deep structures and most data at long periods are 3-D, then 3-D modelling is necessary to correctly study the electrical properties of the subsurface along this dataset.

### 3. Three-dimensional geoelectrical model

Dimensionality analysis indicated that the longer periods of our data cannot be explained by one- or two-dimensional models. Since this study focuses on the deeper structures along the profile, longer periods must be included in our models, so we carried out a 3-D inversion to obtain a suitable electrical model of the subsurface. Although MT data should be ideally disposed on a regular grid for 3-D inversion, there is evidence that 3-D inversion of single profile data, as in our case, may be superior to 2-D inversion (e.g., [Bologna et al., 2017](#); [Meqbel et al., 2016](#); [Tietze and Ritter, 2013](#)). Moreover, since we suspect the existence of a conductor outside of our profile, the use of the full impedance tensor becomes mandatory because the main diagonal elements  $Z_{xx}$  and  $Z_{yy}$  are sensitive to this kind of structure.

The 3-D inversion was carried out using the ModEM code ([Kelbert et al., 2014](#)). Our preferred model was derived by jointly inverting full impedance tensors and vertical transfer functions (VTF). We included periods in the range 0.1 s – 3276 s, totaling 16 periods, and inconsistent responses were removed from the inversion. We set an error floor of 5% of  $|Z_{xy} Z_{yx}|^{1/2}$  for the impedance tensor components and a constant value of 0.03 for the VTFs. The prior model consisted of a 100  $\Omega$  m half-space and we used a covariance value of 0.3 for all directions (x, y and z) and initial damping factor ( $\lambda$ ) of 10. Data and model grid were rotated to the geographic north (N00°). Because station 03 only recorded the components  $Z_{xx}$ ,  $Z_{yy}$ , and  $T_{zx}$ , it could not be rotated and was excluded from this inversion. We also run an inversion rotating the model and data along station's 03 measurement coordinates (x-axis at N13°W) and present the resultant model as Supplementary Material (Fig. S3).

The medium was discretized into  $72 \times 112 \times 52$  cells in the x, y, and z directions, respectively. Horizontally, the cells in the core of our dataset have a nominal resolution of 6 km. Outside the data region, the

grid was padded with 16 cells in each direction, increasing their width by a factor of 1.3. Vertically, the grid is comprised of 52 layers, starting from 25 m and increasing the thicknesses by a factor of 1.2. The final model reached an nRMS of 1.29 after 84 iterations.

[Figs. 6 and 7](#) present horizontal depth slices and vertical cross-sections, respectively, and [Fig. 8](#) presents the final nRMS at each MT station. The model fits well the data in most stations, with an nRMS < 2 in all components. The lowest misfits occur in the  $Z_{xy}$  and  $Z_{yx}$  impedance elements. A comparison between the observed and calculated apparent resistivity and phase curves is shown in the Supplementary Material (Fig. S4). Coast effects were not observed in our data (see Supplementary Material, Figs. S5A and S5B, for details).

The vertical cross-sections ([Fig. 7](#)) show a shallow conductive layer (~10  $\Omega$  m) that can be seen in the entire profile, with depths less than 1 km to the west and reaching up to 5 km depth to the east. Although it appears truncated, this probably occurs due to the low data resolution, since the average data spacing (25 km) is much greater than the depth of the layer. However, our focus lies on lithospheric-scale structures. Two units with resistive crusts and upper mantles (~ $10^3 \Omega$  m until ~120 km), R1 to the west, and R2 to the east, are separated by the crustal conductor C1 (<10  $\Omega$  m, below 15 km).

Conductor C1 (~1  $\Omega$  m) occurs between stations 05 and 06 at approximately 15 km depth ([Fig. 7](#)). A series of smaller neighboring crustal conductors branch out from C1, as seen in the horizontal slices ([Fig. 6](#)). The horizontal slices show that C1 continues outside the profile parallel to its eastern portion. Although off-profile structures should be taken with care, the existence of this conductive lineament is supported by the induction arrows and the dimensionality analysis ([Sections 2.2 and 2.3](#)). Moreover, this conductive anomaly is a robust feature that appeared in all our inversion tests using different rotation angles, initial models, and errors. We relate C1 to a conductive lineament previously

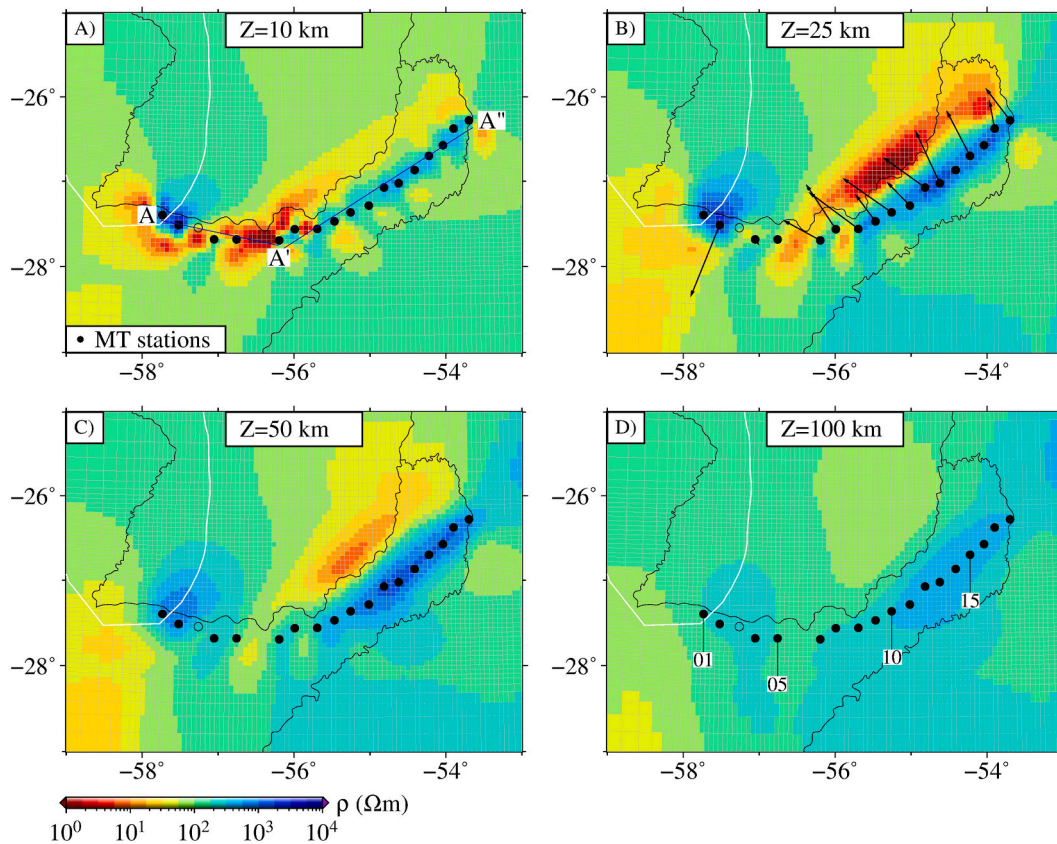


**Fig. 6.** Final 3-D inverse model at representative depths: (a) 10 km, (b) 25 km, with real induction arrows for the period 409.6 s, (c) 50 km, and (d) 100 km. Blue lines in (a) are the cross-section path as seen in [Fig. 7](#). (For interpretation of the references to colour in this figure legend, the reader is referred to the web version of this article.)

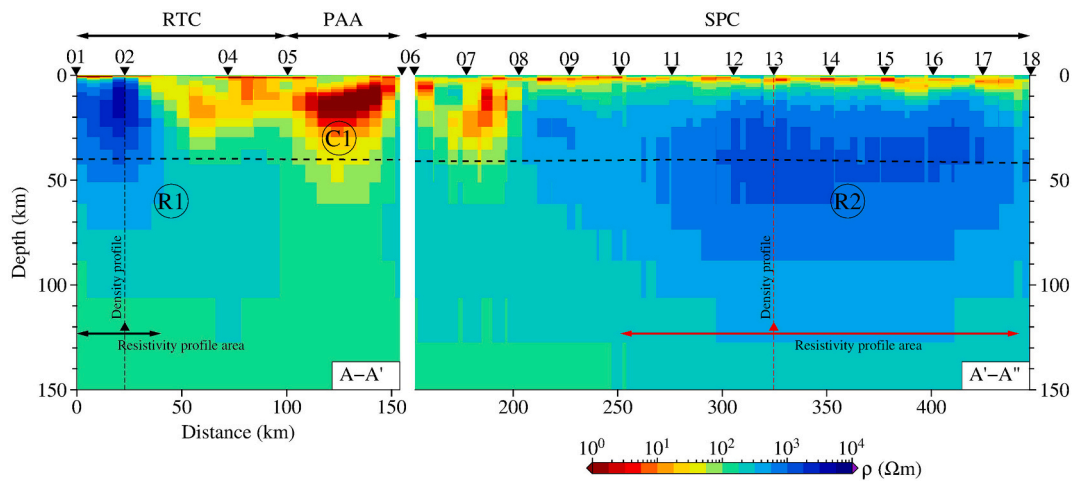


**Fig. 7.** Final 3-D inverse model cross-sections along the MT stations (blue lines shown in Fig. 6a). The dashed black line is the Moho depth (Rivadeneira-Vera et al., 2019). RTC is the Rio Tertiary craton, PAA is the Paraná Axial Anomaly and SPC is the Southern Paraná craton. Density profiles shown in Fig. 10 are taken along stations 02 and 13, whereas the resistivity profiles also shown in Fig. 10 are averaged over the resistivity core of R1 and R2 units, as indicated by the arrows in the cross-sections. (For interpretation of the references to colour in this figure legend, the reader is referred to the web version of this article.)

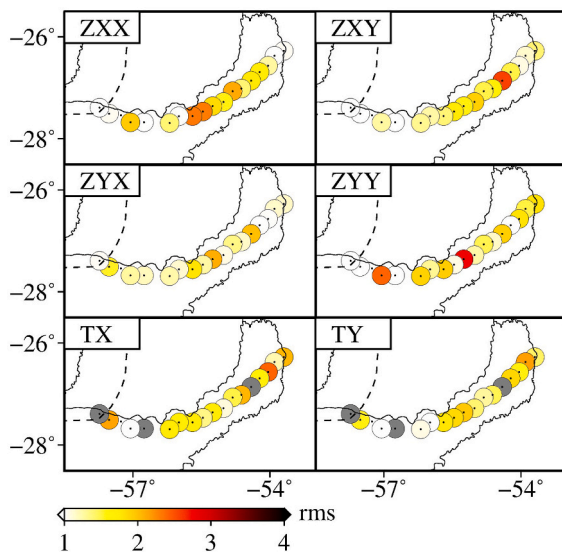


**Fig. 8.** Final 3-D inverse model nRMS for each component of each station. Colored circles are the nRMS averaged over all periods. Gray circles are used where the component was unavailable for that station.

mapped in Brazil and named Paraná Axial Anomaly, discussed in Section 4.1.

Resistor R1 is located beneath the Chaco-Paraná basin, covered with Andean Quaternary deposits at the surface. Its upper crust is highly resistive, above  $3 \cdot 10^3 \Omega \text{ m}$ , while its lower crust and upper mantle are less resistive, between  $3 \cdot 10^2$  and  $5 \cdot 10^2 \Omega \text{ m}$ . From the west, the resistive upper crust is limited past station 02, whereas the upper mantle reaches station 05, giving it a dipping characteristic towards C1. Resistor R2 is located beneath the Paraná basin, filled in the surface by the Mesozoic magmatic rocks. This resistive feature begins at station 08, where a minor crustal conductor related to C1 ends, and continues seamlessly to the east, with a similar electrical lithosphere in the whole area. The upper crust is not as resistive as R1, but the mid to lower crust and upper mantle are more resistive ( $>10^3 \Omega \text{ m}$ ) than R1. Resistors R1 and R2 are related to the Rio Tertiary and Southern Paraná cratons, which are individually and respectively discussed in Sections 4.2 and 4.3, and compared in Section 4.4.

## 4. Discussion

### 4.1. Conductor C1: Paraná axial anomaly

#### 4.1.1. Physical properties and tectonic meaning

Observations supporting that C1 is not only restricted within Argentina but also continues into Brazil are discussed here. First, and most directly, is the geographical coincidence between C1 and a conductive lineament mapped in Brazil in previous induction studies (Fig. 9a). The possibility of a conductive lineament beyond the Brazilian borders was first pointed out by Bologna et al. (2014). They observed a series of reversions in GDS (Geomagnetic Deep Sounding) induction arrows that occur close to the Paraná basin depocenter, reaching the Brazilian-Argentinian border. These reversions were interpreted as indicative of an elongated conductive feature trending approximately NNE-SSW. Later, Padilha et al. (2015), combining 3-D inversion of the GDS data and 2-D inversion of an MT profile, imaged a crustal conductive lineament bounded by induction arrow reversions (Fig. 9b). Maurya et al. (2018) refined this result using additional MT stations in the central Paraná basin and running a 3-D joint inversion of MT and GDS data. They named this lineament Paraná Axial Anomaly (PAA) due to its occurrence along the Paraná basin axis. Both studies already observed a conductor in northeastern Argentina; however, due to lack of data, it appeared isolated and at different depths (see the beginning of profile C1-C2 in Padilha et al., 2015, Fig. 7, and Maurya et al., 2018, Fig. 12).

Second, C1 conductor and PAA share geophysical properties. In the electrical models, the PAA is confined to the mid-crust (15–20 km, see Maurya et al., 2018), similar to C1 average depth (Fig. 7). The intensities of conductors C1 and PAA are also similar, close to  $1 \Omega \text{ m}$ . In addition to the electrical properties, PAA is coincident with a NE-SW trending gravity high in the center of the Paraná basin observed in the SAGM04 gravity model (de Sá, 2004; Fig. 9c), and it is also coincident with positive magnetic anomalies observed in the NGDC-270 model (Maus, 2010; Fig. 9d). These characteristics continue along C1 path.

Third, both C1 and PAA occur in areas of thickest basalt accumulation ( $>1 \text{ km}$ ). Correlation between PAA and thick basalt zones is evident in Brazil, where the stratigraphy of the volcano-sedimentary rocks is constrained by several wells drilled by the oil industry. However, the same information is not available in Argentina, especially in the province of Misiones (e.g., Pezzi and Mozetic, 1989). To compensate for this lack of drilling data, we performed 1-D inversion of our MT data using the IPI2Win software (Bobachev, 2002, see Supplementary Material,

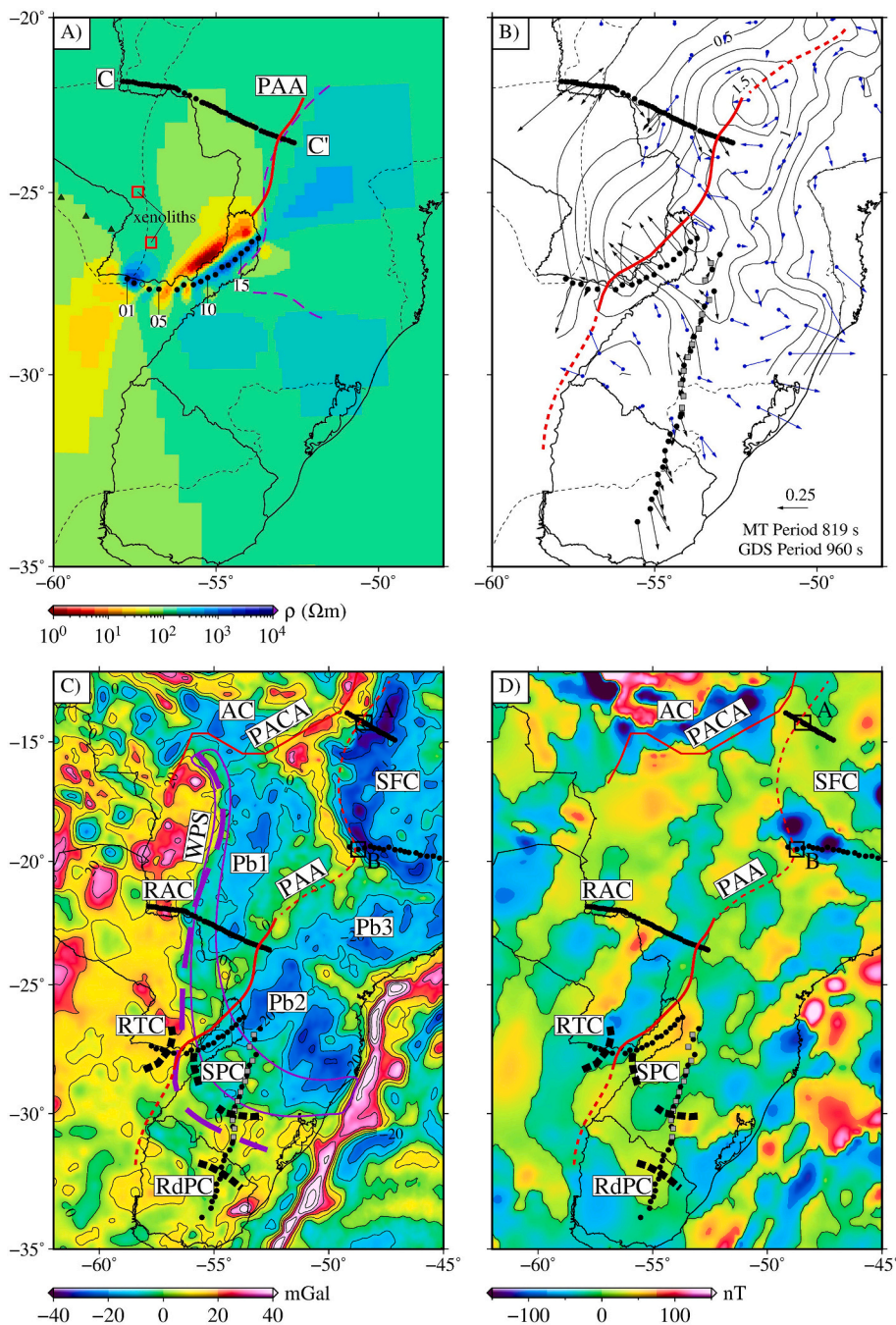


Fig. S6). We used the rotationally invariant response derived from the arithmetic average of the off-diagonal MT impedances (Ingham, 1988) as input and re-interpolated the basalt isopach map for the Paraná and Chaco-Paraná basins (Fig. 9b). The maximum thickness ( $\sim 1.5$  km) is observed in Brazil along a NE-SW trending direction to the east of the Paraná River and coincident with the PAA location. This trend continues into Argentina, where thicknesses between 1.5 and 1.0 km occur between stations 18 and 12, from east to west. The basalt layer thickness decreases westwards as it approaches resistor R1. The mass excess caused by the basalt layer correlates with the gravity high that coincides with both PAA and C1 (Fig. 9c).

These observations reinforce that conductor C1 is a continuation of PAA. Based on E-W conductive anomalies in the southern Paraná basin, Maurya et al. (2018) have suggested that the PAA modeled in the central Paraná basin would bend to the east towards the Torres syncline

Fig. 9. (a) 3-D inversion model at 25 km. The red line is the crustal conductor published by Padilha et al. (2015) modeled from GDS data and MT profile C-C'. The dashed purple line is the PAA published by Maurya et al. (2018). Red squares are sites of sampled mantle xenoliths (Comin-Chiaramonti et al., 2010). Green triangles are MT stations from Favetto et al. (2015). (b) Induction arrows and basalt thickness isopachs at 250 m intervals. The map was interpolated using minimum curvature splines (Smith and Wessel, 1990; more details on 1-D inversion are given as Supplementary Material, see Fig. S6 and Table S1). The solid red line shows the new PAA trace proposed in this study. Dashed red lines show the possible extension of the PAA to the south, based on published GDS data, thickness of the Serra Geral basalts, and gravity. (c) Residual gravity map obtained from the difference between Bouguer anomalies from the SAGM04 gravity model (de Sá, 2004) upward continued to 10 km and a regional field upward continued to 100 km. Pb1, Pb2 and Pb3 are different gravity domains inside the Paraná basin. The solid purple line is the WPS by Dragone et al. (2017), whereas the dashed purple is the revised WPS trace (Section 4.3). (d) Magnetic anomaly map from NGDC-720 (Maus, 2010). Common to (c) and (d): thick dashed black are limits of the tectonic units based on MT data: RdPC (Bologna et al., 2019), RTC, and SPC (this work). Squares A and B are locations of mid to lower crustal and/or upper mantle conductive anomalies in other MT studies (A – Padilha et al., 2013; B – Bologna et al., 2011). Other abbreviations: AC – Amazon craton; PACA – Paraguay-Araguaia Conductive Anomaly; RAC – Rio Apa craton; SFC – São Francisco craton. (For interpretation of the references to colour in this figure legend, the reader is referred to the web version of this article.)

following the WPS (see Figs. 1 and 9a). This eastward bending (see Fig. 9a) is now probably ruled out. PAA follows the Argentinian-Paraguayan border (the Paraná River) until  $56.5^\circ\text{W}$ , close to the eastern border of resistor R1, where it bends to the south. PAA, including C1 found in this study, may reach at least 800 km (see red line in Fig. 9b).

Low resistivity values such as those observed for the PAA are not common in the mid-crust of stable areas because dry silicate rocks are usually highly resistive. Since the last tectono-magmatic event occurred in the Late Cretaceous and considering that heat flow measurements in the central Paraná basin restrain the temperatures below the mantle solidus, Padilha et al. (2015) ruled out fluids and partial melts to explain the low resistivities observed in the conductor within the Paraná basin. The origin of the anomaly was thus ascribed to interconnected mineral phases, which in turn were related to the Serra Geral flood volcanism,

since the conductive lineament coincides with the maximum basalt thickness in the basin (cf. Fig. 9b). Spatial correlation between the conductive lineament and magnetic anomalies observed in the NGDC-270 global model (Maus, 2010; see Fig. 9d) restrained the minerals among those with high susceptibility, such as iron sulfides and iron oxides precipitated during magmatic extrusion.

Iron-bearing minerals may not be the only explanation for the conductive anomaly, however. Evans (2012) states that Fe–Ti oxide gabbros have only been observed to occur as localized intrusions of evolved magmas in oceanic crust and cannot increase the bulk conductivity on a scale measurable by MT. The large volume of basalts in our case differs from their example and may be the reason for the high conductivity. Nevertheless, another possible explanation for the high conductivity is the tectonic scenario of PAA as a fossil suture zone. The interpretation of PAA as a suture zone will be further discussed in Section 4.5 and was proposed by Dragone et al. (2017), following Milani and Ramos (1998) idea of the Paraná basin lithosphere being formed by the assemblage of several cratonic nuclei and terranes. In this case, the conductivity could have been increased through the presence of sulfides or graphite in metasediments that were trapped in the crust during subduction and ocean closure. Conductive lineaments with dimensions similar to PAA are usually associated with sutures, such as the PACA (Paraguay-Araguaia Conductive Anomaly) lineament in the southern limit of the Amazon craton (Bologna et al., 2014) or the NAPC (North American Central Plains) anomaly along the Trans-Hudson Orogen, between the Wyoming/Rae-Hearne and Superior cratons (Jones et al., 2005).

#### 4.1.2. Possible PAA extensions

The PAA may continue further to the south inside Argentina. Induction arrows at several GDS stations in southern Brazil, between latitudes 28°S and 30°S, point to the west/northwest (Fig. 9b, see also Bologna et al., 2014). This response would be compatible with a conductive structure within Argentina running in the N–S direction. Also, an MT study at the border between Argentina and Uruguay (Corbo et al., 2012) shows that there is a > 1 km basalt layer to the west of the Uruguay River. If the PAA has a causal relation with the magmatic extrusion, we can hypothesize that the conductive anomaly continues there. Confirmation of this extension requires additional geophysical data, but, if correct, then the PAA could mark the Rio de la Plata craton western limit (Fig. 9b).

To the north, a similar correlation with maximum basalt thickness suggests a continuation of the PAA until 20°S latitude and 49°W longitude (Fig. 9b). The associated gravity lineament (Fig. 9c) continues towards the Brasília belt, the southwestern limit of the São Francisco Craton, where it bends to the NNW towards the PACA lineament (Bologna et al., 2014). It then bends towards the NE, bordering the São Francisco craton over the Brasília belt. Since the reversion pattern in the GDS induction arrows is no longer observed at these latitudes, further investigation of this possible northward extension of PAA should be carried out in the future to test this hypothesis.

This northern extension of the PAA is coincident with conductive anomalies associated with suture zones (squares A and B in Fig. 9c and d) observed in other induction studies (Bologna et al., 2011; Padilha et al., 2013). This relationship is further explored in Section 4.5.

#### 4.2. Resistor R1: Rio Tebicuary craton

Resistive feature R1 is concealed by 1 km-thick Chaco-Paraná basin sedimentary rocks. The underlying tectonic unit of the Chaco-Paraná Basin is usually ascribed to the Rio de la Plata craton (Almeida et al., 1973), initially limited by Paleoproterozoic outcrops in the Piedra Alta terrane of Uruguay, Tandilia belt of Argentina, and Taquarembó block in southern Brazil (Fig. 1). Since the craton is mostly concealed by sedimentary deposits, the geometry of the tectonic fabric under the basin has been changed over the years, based both on geological (e.g. Oriolo et al.,

2016; Oyhantçabal et al., 2011; Rapela et al., 2011, 2007) and geophysical studies (e.g. Bologna et al., 2019; Dragone et al., 2017). Associating a resistive lithosphere ( $>10^3 \Omega \text{ m}$ ) observed in MT studies carried to the west of our study area (Favetto et al., 2015, 2008; Orozco et al., 2013; Peri et al., 2015, 2013) with a circular gravity high ( $>0 \text{ mGal}$ ), Dragone et al. (2017) suggested a distinct resistive cratonic lithosphere under the Chaco-Paraná basin, the Rio Tebicuary craton.

The Rio Tebicuary craton is exposed in southern Paraguay in the Paleoproterozoic Villa Florida Metamorphic Suite (Fig. 1), with U–Pb ages of  $2023 \pm 12 \text{ Ma}$  (Cordani et al., 2001) and between  $2240 \pm 20 \text{ Ma}$  and  $2040 \pm 30 \text{ Ma}$  (Lohse, 1990, apud Leite et al., 2018). The zero mGal contour that limits the craton (see Fig. 2b) crosses our MT profile between stations 04 and 05, located on the eastern end of resistor R1. We thus interpret R1 as the eastern border of the Rio Tebicuary craton (Fig. 9c). To the west, the craton is limited by the Pampia terrane (Favetto et al., 2015, and references therein), and to the east by the PAA (C1) between stations 05 and 06.

Our 3-D inversion model shows that the crust at the eastern border of the Rio Tebicuary craton reaches values higher than  $3 \cdot 10^3 \Omega \text{ m}$ , whereas its upper mantle resistivity is between  $3 \cdot 10^2$  and  $5 \cdot 10^2 \Omega \text{ m}$ . These values are similar although slightly lower in comparison to those observed to the west. In Favetto et al.'s (2015) final model, whose MT stations are closest to ours (see Fig. 9a), the crust reaches values above  $5 \cdot 10^3 \Omega \text{ m}$  and the upper mantle above  $10^3 \Omega \text{ m}$ . High resistivities are compatible with a cratonic lithosphere, since cratons are portions of the continent that remained tectonically stable for long periods of time, favoring the absence of partial melts and fluids (Selway, 2014). High resistivities are observed in other cratons around the world, such as the Congo craton in Africa (Khoza et al., 2013), and the Wyoming (Meqbel et al., 2014) and Superior (Yang et al., 2015) cratons in North America. The slightly lower resistivities found in our model when compared to that of Favetto et al. (2015) are probably related to a metasomatic process that may have affected the upper mantle in the eastern border of the Tebicuary craton (see Section 4.4).

Positive Bouguer anomalies associated with cratonic and electrically resistive lithospheres also occur in the Rio Apa (Padilha et al., 2015) and Rio de la Plata (Bologna et al., 2019) cratons. All of them are marked by normal to thin crust ( $<35 \text{ km}$ ), as discussed by Dragone et al. (2017), and exhibit the same electrical distribution: an upper crust with high resistivity ( $>10^3 \Omega \text{ m}$ ) and lower crust and subcontinental lithospheric mantle (SCLM) slightly less resistive ( $5 \cdot 10^2$  to  $10^3 \Omega \text{ m}$ ). The unexpected correlation between cratons and gravity highs will be further discussed in Section 4.4.

#### 4.3. Resistor R2: Southern Paraná craton

The highly resistive lower crust and upper mantle ( $>10^3 \Omega \text{ m}$ ) observed for R2 suggest a cratonic lithosphere, as previously discussed for R1. An MT study to the east of our profile comprising data gathered between central Uruguay and Santa Catarina in Brazil has shown similar electrical characteristics for the lithosphere of the southern Paraná basin (Bologna et al., 2019). Their model shows high resistivities ( $>10^3 \Omega \text{ m}$ ) from crustal depths (25 km) down to the upper mantle (100 km), as observed in our geoelectrical model (Fig. 7). To further investigate these similarities, we run a 3-D inversion combining their data with those presented in this paper. The resultant electrical model, shown in the Supplementary Material (Fig. S7), confirms that the lithospheres beneath both datasets are similar. Henceforth, we name R2, including the area to the east, Southern Paraná craton (see limits in Fig. 9c and d).

Interpretation of this unit as cratonic also finds support on seismological data. Rocha et al. (2019), using teleseismic P-wave tomography, mapped a region of high velocity at 200 km depth coincident with the Southern Paraná craton. Their interpretation, however, extended beyond these limits and included most of the Paraná basin in a single cratonic block, which is not supported by MT data.

The contact between the Rio Tebicuary and the Southern Paraná

cratons lies within a lithospheric transition zone, the WPS, a Neoproterozoic-Cambrian suture or shear zone, proposed by Dragone et al. (2017). The gravity gradient on the western and southern boundaries of the Paraná Basin is the geophysical signature used to delimit the WPS. The new MT data now show that the lithospheres are also electrically distinct, and we will further explore this difference in the next Section 4.4.

The WPS as originally proposed lies within the new unit Southern Paraná craton (see purple line in Fig. 9c). This result led us to revise the WPS trace in the transition between the Southern Paraná and Rio de la Plata cratons, which must lie further to the south. This change in the WPS trace fits better the gravity residual when the gravity components due to large wavelengths, such as those from crust thickness variation, are removed (see details in Fig. 9c), and it is also in accordance with a recent seismological study in the region by Shirzad et al. (2020). Using ambient seismic noise, they show that variations in velocity propagation in the crust occur, from north to south, closer to the newly proposed WPS trace at latitude 30°S.

#### 4.4. Electrical resistivity and density: Constraining lithosphere composition

The geoelectrical cross-section in Fig. 7 shows the PAA and the WPS separating two lithospheres with distinct resistivity distribution, the Rio Tebicuary craton (RTC) to the west and the Southern Paraná cratonic block (SPC) to the northeast. In the RTC, the entire crust is highly resistive ( $>10^3 \Omega \text{ m}$ ) and below the Moho the upper mantle resistivity decreases rapidly to  $100 \Omega \text{ m}$  at  $\sim 200 \text{ km}$  depth. In the SPC, most of the upper crust is conductive to moderate resistive and more resistive ( $>10^3 \Omega \text{ m}$ ) in the lower crust and upper mantle. Then, it steadily decreases reaching  $100 \Omega \text{ m}$  value at  $\sim 300 \text{ km}$  depth. These geoelectrical vertical profiles are summarized in Fig. 10 together with an independent density contrast distribution as a function of depth for both cratons. The locations of the density profiles coincide with two MT stations and the resistivity profiles are constructed estimating an average value along a horizontal slice at a fixed depth interval, as shown in Fig. 7.

We adopted  $100 \Omega \text{ m}$  as an upper limit for the electrical LAB (lithosphere-asthenosphere boundary). This value is within the laboratory determined conductivity ( $\sim 10^{-2} \text{ Sm}^{-1}$ ) observed for dry olivine at mantle conditions (Xu et al., 2000b, 2000a). It also matches the resistivity observed at depths of 200–300 km in long-period MT experiments focused on the study of the deep continental mantle (e.g. Olsen, 1999; Tarits et al., 2004).

Bouguer gravity anomalies as shown in Fig. 2(b) and Fig. 9(c) also indicate distinct density distributions for both cratonic lithospheres. We will speculate about the composition and the age of the SCLM by adding density as an additional physical information.

The density model for the Paraná magmatic province and surrounding tectonic provinces was estimated from geoid anomalies (Chaves et al., 2016). Whilst Bouguer gravity is more sensitive to mass anomalies within and at the base of the crust, geoid anomalies are also sensitive to density variations within the upper mantle and below (Chaves and Ussami, 2013). The depth dependent density contrast for RTC and SPC are shown in Fig. 10, together with their electrical resistivities. Density contrast is the departure of the geoid anomalies estimated density from the mean densities of the crust and the mantle with depth. RTC and SPC have contrasting density profiles. The RTC lithosphere is, in average, denser and thinner than the SPC lithosphere. This explains why Bouguer anomalies in the RTC are more positive whereas in the SPC they are dominantly negative (Fig. 9c).

According to Poudjom-Djoman et al. (2001) and Griffin et al. (2009), direct density measurements of peridotite xenoliths sampled from main SCLMs in the world indicate a secular variation in crustal and SCLM composition and its density. At  $20^\circ \text{C}$ , the Primitive Mantle (asthenosphere) density is approximately  $3390 \text{ kg/m}^3$  and it decreases with age, the Archean SCLM density being the lowest ( $3310 \pm 160 \text{ kg/}$

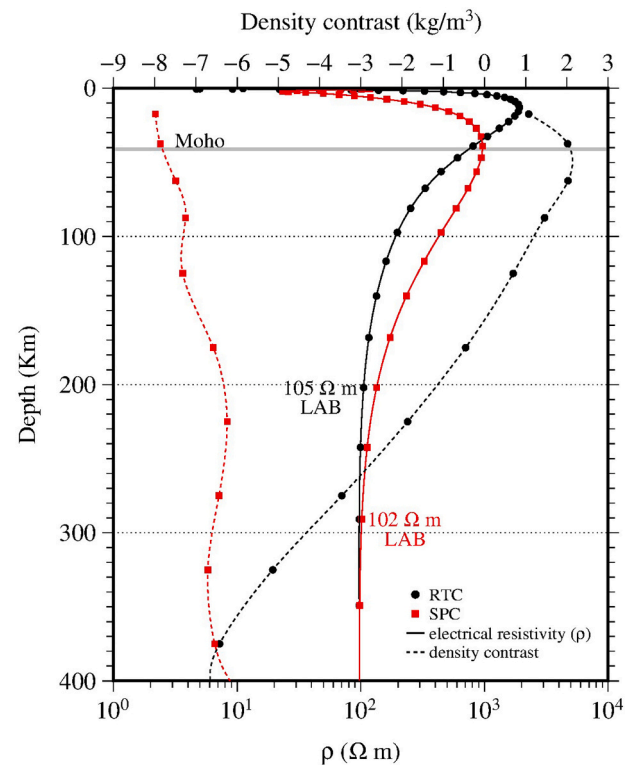


Fig. 10. Vertical depth profiles of electrical resistivity (this work, solid lines) and density contrast after 3-D linear inverse modelling of geoid anomalies (Chaves et al., 2016, dashed lines) for two cratonic lithospheres, the Rio Tebicuary (RTC, in black) and the Southern Paraná (SPC, in red) cratons. Electrically defined lithosphere-asthenosphere boundary (LAB) is assumed to be at  $100 \Omega \text{ m}$  resistivity (see text for details). (For interpretation of the references to colour in this figure legend, the reader is referred to the web version of this article.)

$\text{m}^3$ ), followed by Proterozoic ( $3350 \pm 20 \text{ kg/m}^3$ ) and Phanerozoic ( $3360 \pm 20 \text{ kg/m}^3$ ) SCLMs. As age increases the SCLM becomes more depleted of Al, Ca, #Mg and Fe/Al. The magnesium number #Mg is defined as the ratio  $\text{Mg}/(\text{Mg} + \text{Fe})$ . Lee (2003) correlated seismic velocities and density with #Mg and SCLM composition because this parameter reflects the inverse of the amount of Fe in peridotite. The higher the #Mg, the lower its density.

As shown in Fig. 10, in SPC the SCLM vertical profile has negative density contrast from crust to mantle and its corresponding resistivity curve indicates a thick ( $> 200 \text{ km}$ ), cold and dehydrated cratonic lithosphere, characteristic of an Archean or Paleoproterozoic SCLM (Griffin et al., 2009).

In opposition, RTC presents a positive density contrast down to 150 km which correlates with a resistive SCLM. As described in Section 4.2, basement crustal rocks in RTC are dated as Paleoproterozoic (Cordani et al., 2001; Lohse, 1990, apud Leite et al., 2018), likewise its SCLM if they both evolved under the same tectono-thermal history. According to Griffin et al. (2009) for Paleoproterozoic SCLM, as the case of RTC, the density is expected to be proximal to a depleted and less dense Archean SCLM. However, this is not the case, RTC is denser as estimated from gravity (geoid) anomalies. Also, a study by Comin-Chiaromonte et al. (2010) on mantle xenoliths and xenocrysts brought to the surface by Cenozoic alkaline magmatism in Eastern Paraguay gives direct evidence on SCLM density. The Misiones samples (see location in Fig. 9a) near Argentina border and close to the MT soundings are xenoliths composed of mainly spinel-lherzolites, harzburgites and subordinate dunites. The xenoliths are low-K and their #Mg are  $\sim 0.87$ .

Griffin et al. (2009) have obtained #Mg values  $> 0.91$  in depleted Archean cratons (examples Kaapvaal, East Greenland, Tanzania) and

density range of  $\sim 3335 \text{ kg/m}^3$ . In Proterozoic cratons density is  $\sim 3360 \text{ kg/m}^3$  and  $\#Mg \sim 0.91$ . Therefore,  $\#Mg$  values observed in RTC predicts mantle composition and density typical of a primitive mantle (or asthenospheric). Comin-Chiaramonti et al. (2010) suggests metasomatic processes in RTC mantle which may have increased its density with time. As observed in the Southern Archean Churchill Province (Boerner et al., 1999), metasomatism can enhance the electrical conductivity of the SCLM and, therefore, explain the slightly less resistive root in the RTC relative to the SPC.

Another possible explanation for the differences in the gravity signature between the RTC and SPC is related to the genesis of these continental crusts, where hot spot tectonic processes as described by Fyfe (1978) could generate a more mafic and thus a denser crust, resulting in the positive Bouguer anomalies observed for the RTC. This alternative hypothesis is discussed in more detail in Dragone et al. (2017).

#### 4.5. SW Gondwana assembly and the age of PAA

The PAA proposition and its possible extensions together with the delimitation of cratonic units in this study allow us to review the tectonic history of SW Gondwana and set a minimum age for the suture.

We set the Paraná basin as the center of convergence for the surrounding units. Regarding the basin lithosphere, Dragone et al. (2017) interpreted a series of circular negative Bouguer anomalies that occur

within it as the geophysical signatures of small cratonic nuclei or terranes. However, interpretation of gravity lows as cratonic nuclei or terranes in the Paraná basin is not always direct and integration with other methods are necessary. For example, an MT study in the north-western basin shows a gravity low associated with a conductive anomaly that was interpreted as a lithospheric discontinuity between cratonic segments (Bologna et al., 2013). A full characterization of the Paraná basin lithosphere is beyond the scope of this study. However, integrating the existent geophysical data we observe that the Paraná lithosphere is heterogeneous and can be roughly segmented according to the Bouguer anomalies shape and intensity. The gravity high coincident with the PAA separates its western and eastern gravity domains (respectively Pb1 and Pb2/Pb3 in Figs. 9c, 11a), and each domain is composed of cratonic fragments, terranes, and sutures.

As previously discussed in Section 4.1.1, the PAA may be associated with a fossil suture zone. This suture was reactivated in the Silurian-Ordovician, controlling the initial subsidence of the Paraná basin during the syn-rifting phase, as proposed by Milani and Ramos (1998). A similar process of subsidence driven by the suture could also have occurred in the initial phases of the Chaco-Paraná basin evolution. The coincidence of the PAA with the maximum basalt thickness also suggests that the same crustal/lithospheric discontinuity was reactivated during the Early Cretaceous Serra Geral flood volcanism, acting as the main area for basalt extrusion as formerly proposed (Maurya et al., 2018; Padilha et al., 2015).

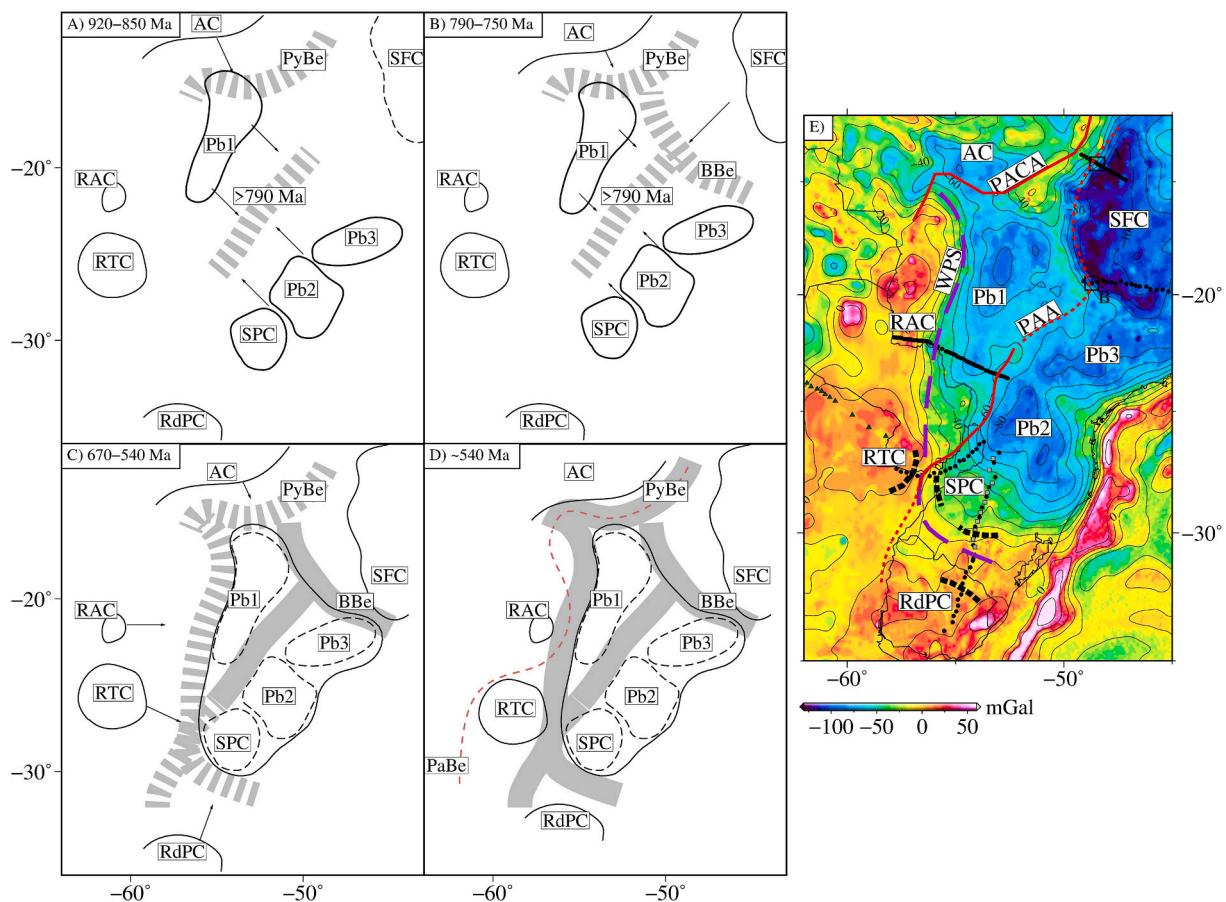


**Fig. 11.** Tectonic evolution of the Paraná basin and its surrounding units (ages in box). (a) Onset of convergence between the Amazon craton (AC) and Paraná basin lithosphere (PB) along the (present day) Paraguay belt (PyBe). The PB also results from cratons/terrane amalgamated before/during this convergence. Dashed grays are regions of suture/ocean closures. (b) Onset of convergence between the São Francisco craton (SFC) and PB along the (present day) Brasília belt (BBE). (c) Onset of convergence between Rio Apa (RAC), Rio Tebicuary (RTC), and Rio de la Plata (RdPC) cratons towards the PB along the WPS. Solid grays depict regions already closed. (d) Final units' assembly. The dashed red line is the Clymene ocean (cf. Tohver et al., 2012). PaBe is the Pampean belt. (e) Bouguer anomaly map with present-day limits. Solid red is the PAA constrained by MT and GDS data. Dashed reds are the PAA extensions based on other geophysical data. Dashed purple is the revised WPS. (For interpretation of the references to colour in this figure legend, the reader is referred to the web version of this article.)

In order to set a possible age for this suture and whether it continues beyond the limits of the Paraná basin, we compiled the ages of exposed sutures together with gravity data and former MT studies. Fig. 11 is an attempt to restore the chronology and paleogeography of the SW Gondwanaland amalgamation. To the north, according to Pimentel and Fuck (1992), the region between the Amazon and São Francisco craton and the Paraná basin lithosphere, known as Tocantins province, was formed by a progressive accretion and amalgamation of island arcs followed by the Goiás-Pharusian ocean closure and continental collision, observed in linear swarms of ophiolitic bodies in the Arenópolis and Iporá volcano-sedimentary suites.

Initial convergence between the Amazon and São Francisco cratons is observed in the 900–850 Ma meta-tonalite of Arenópolis and Mara Rosa and the c. 920 Ma Arenópolis rhyolitic rocks (Pimentel et al., 2000). These are the earliest records of convergence in the region (Fig. 11a). At 790 Ma, collisional magmatism is observed only in the southern portion of the Brasília Belt, probably marking the onset of the collision between the Paraná lithosphere and the São Francisco craton. For this tectonic setting, the cratonic nuclei or terranes that comprise the Paraná lithosphere must have formed a single unit by the time of, or before, the collision against the São Francisco craton, so we assume that this closure is older than 790 Ma (Fig. 11b).

Several areas of the Tocantins province present metamorphic ages of 630 Ma. This metamorphism is thought to result from the collisional event that sets the final closure of the Goiás-Pharusian ocean in the region, as shown in Fig. 11(c). Other studies suggest different ages for the final closure. Frugis et al. (2018) consider that the final ocean closure happened at 670 Ma, which is the limit age for the deposition of the syn-collisional unit Serra da Boa Vista. On the other hand, paleogeographic reconstructions based on paleomagnetic studies, suggest a later closure between 550 and 500 Ma along the Clymene ocean (Tohver et al., 2012; Trindade et al., 2006). Clymene closure path encompasses three belts, Araguaia to the north (not shown), Paraguay in its central portion, and Pampean to the south (Fig. 11d).

These sutures are observed in MT profiles that cross the gravity gradient between the Brasília belt and the São Francisco and Amazon cratons. The gradient area is usually accompanied by conductive anomalies in the mid to lower crust and/or upper mantle modeled from MT data (see squares A and B in Fig. 9c and d). One of the possible explanations for Profile A (Padilha et al., 2013) conductive anomaly is the subduction of an oceanic lithosphere. The source of the conductivity, in this case, was ascribed by the authors to organic carbon deposited in the ocean floor and later metamorphized and introduced in the mantle during Neoproterozoic subduction. This subduction scenario is evidenced by the presence of the Goiás magmatic arc and metamorphosed ophiolitic mélanges in the Brasília belt. Profile B (Bologna et al., 2011) conductive anomaly is associated with the same process of organic material from an organic-rich basin underthrust during a suture process between the São Francisco craton and the Paraná basin lithosphere in the Neoproterozoic.

To the south and west of the Paraná lithosphere, Dragone et al. (2017) observed that syn-collisional granites of ~540 Ma occurs along a gravity gradient between the Paraná basin and the surrounding cratonic units Rio de la Plata, Rio Tebicuary, and Rio Apa. This was interpreted as the closure age between these cratons and the Paraná lithosphere, as shown in Fig. 11(d). The limit between the Rio de la Plata and Rio Tebicuary cratons could be that of a shear zone or a suture between these units, possibilities that should be further investigated. And the limit between the Rio de la Plata and Southern Paraná craton comprises a succession of subductions towards the Paraná basin, as discussed in Bologna et al. (2019).

The SW Gondwana assembly, as we propose in Fig. 11, depicts the heterogeneous Paraná lithosphere as a center of convergence of several tectonic units from all sides as well as along the PAA. These sites are associated with subduction processes, where the subducting slab releases fluids and enriches the mantle wedge, and the lithospheric mantle

above it, with incompatible elements. The chemical and isotopic composition of Paraná-Etendeka LIP basalts has always been associated with the melting of an enriched and heterogeneous SCLM (Marques et al., 1999; Peate et al., 1992; Piccirillo et al., 1989). This enrichment may be one of the reasons for the large basalt volume extruded and why it is confined mostly inside the Paraná basin, decreasing towards the Chaco-Paraná basin/Rio Tebicuary craton. More recently the use of Os—Os systematic has also found asthenospheric components from mantle wedge in basalts of northern Paraná province (Rocha-Júnior et al., 2013). Basalts were also generated from melting of SCLM distinct in composition and age as shown by Rocha-Júnior et al. (2020). This demonstrates the importance in integrating the geophysical methods to decipher the three dimensional physical and composition structure of the lithosphere and its role in the genesis of the LIP.

## 5. Conclusions

The MT survey carried out in this study has shown thick and resistive lithospheres with cratonic affinity (cold, dry, and stable) beneath the Chaco-Paraná and southern Paraná basins. The basement of the Chaco-Paraná in this area is the Rio Tebicuary craton. We could now establish its eastern limit towards the Paraná basin. We could also propose that the Paraná basin basement is cratonic in its southern portion, which we referred to as Southern Paraná craton. However, gravity, electrical, and compositional heterogeneities do not support the idea of a single craton encompassing the entire Paraná basin. Although both cratons are overall resistive, they have distinct electrical and density profiles with depth. The higher-than-expected density of the Paleoproterozoic Rio Tebicuary craton lithosphere may be explained by metasomatic processes as suggested by geochemical data of peridotitic xenoliths. The same metasomatic process may also explain the relatively lower resistivity at the Rio Tebicuary SCLM when compared to the Southern Paraná craton. Alternatively, a higher density in the Rio Tebicuary craton could also be explained by a hot spot tectonic process to generate its continental crust, resulting in a higher concentration of mafic material in the crust and upper mantle.

Our electrical model also shows that the Rio Tebicuary and Southern Paraná cratons are separated by a crustal conductive lineament named Paraná Axial Anomaly (PAA). The PAA is a lithospheric discontinuity previously mapped in the Paraná basin (Brazil) that we propose to continue into the Chaco-Paraná basin (Argentina). PAA is a suture zone we dated as Early Neoproterozoic based on SW Gondwana reconstruction and several ocean closures by this time. This suture controlled the location of the initial subsidence of the Paraná and Chaco-Paraná basins in the Late Ordovician and of the Serra Geral magmatism in the Jurassic-Lower Cretaceous. Basalt thickness, as well as GDS, gravity, and magnetic data, suggest that this lineament could continue further to the south and to the north of areas where it is constrained by induction data. These extensions of the PAA also coincide with conductive zones shown in MT profiles that were interpreted as fossil suture zones. These sutures are associated with subduction zones which favored refertilization processes that enriched the former cratonic and depleted Paraná SCLM, from where tholeiitic basalts may have been later extracted.

The integration of newly acquired MT data with former gravity, magnetic, seismological, and electromagnetics induction studies allowed us to provide a new view on the Paraná and Chaco-Paraná intracratonic basins and their heterogeneous lithosphere, with implications to the tectonic history of the SW Gondwana assembly, the basins evolutions, and the genesis of a LIP.

## Data availability

Magnetotelluric transfer function estimates are available through the Zenodo data repository (doi:<https://doi.org/10.5281/zenodo.3967396>).

## Declaration of Competing Interest

The authors declare that they have no known competing financial interests or personal relationships that could have appeared to influence the work reported in this paper.

## Acknowledgements

Data acquisition was financially supported in Brazil by FAPESP (Thematic Project 2012/06082-6) and CAPES (project CAPES-MINCYT 234/13), and in Argentina by MINCYT (project MINCYT-CAPES BR/12/02). We thank CNPq (152843/2018-3) and CAPES for the G. Dragone post-doctoral scholarships during the writing of this paper. N. Ussami is supported by research grant from CNPq (309506/2015-8). We thank Isac Carneiro dos Santos and Jorge Tapias Simanca for the assistance during field work. Data modelling has made use of the computing facilities of the Laboratory of Astroinformatics (IAG/USP, NAT/Unicisul), whose purchase was made possible by the Brazilian agency FAPESP (grant 2009/54006-4) and the INCT-A. All figures were made using the GMT software package (Wessel and Smith, 1991; Wessel et al., 2013). We thank two anonymous reviewers for their careful and thoughtful comments that helped us to improve this paper.

## Appendix A. Supplementary data

Supplementary data to this article can be found online at <https://doi.org/10.1016/j.tecto.2021.228884>.

## References

- Allen, P.A., Allen, J.R., 2013. *Basin Analysis: Principles and Application to Petroleum Play Assessment*, 3rd edition. Wiley, Oxford.
- Almeida, F.F.M., Amaral, G., Cordani, U.G., Kawashita, K., 1973. The Precambrian evolution of the South American Cratonic margin south of Amazon River. In: Nairn, A.E.M., Stehli, F.G. (Eds.), *The Ocean Basins and Margins*, vol. 1. Plenum Press, New York, pp. 411–446.
- de Almeida, F.F.M., de Brito Neves, B.B., Carneiro, C.D.R., 2000. The origin and evolution of the South American Platform. *Earth Sci. Rev.* 50, 77–111. [https://doi.org/10.1016/S0012-8252\(99\)00072-0](https://doi.org/10.1016/S0012-8252(99)00072-0).
- Amante, C.B., Eakins, W., 2009. ETOPO1 1 Arc-Minute Global Relief Model: Procedures, Data sources and Analysis. NOAA Technical Memorandum NESDIS NGDC-24. National Geophysical Data Center, NOAA. <https://doi.org/10.7289/V5C8276M>.
- Bibby, H.M., Caldwell, T.G., Brown, C., 2005. Determinable and non-determinable parameters of galvanic distortion in magnetotellurics. *Geophys. J. Int.* 163, 915–930. <https://doi.org/10.1111/j.1365-246X.2005.02779.x>.
- Bobachev, C., 2002. *IP2Win: A Windows Software for an Automatic Interpretation of Resistivity Sounding Data (Doctoral Dissertation)*. Moscow State University, Moscow, Russia.
- Boerner, D.E., Kurtz, R.D., Craven, J.A., Ross, G.M., Jones, F.W., Davis, W.J., 1999. Electrical conductivity in the precambrian lithosphere of western Canada. *Science* 283 (5402), 668–670. <https://doi.org/10.1126/science.283.5402.668>.
- Bologna, M.S., Padilha, A.L., Vitorello, Í., Pádua, M.B., 2011. Signatures of continental collisions and magmatic tectonics in Central Brazil as indicated by a magnetotelluric profile across distinct tectonic provinces. *Precambrian Res.* 185, 55–64. <https://doi.org/10.1016/j.precamres.2010.12.003>.
- Bologna, M.S., Nunes, H.O., Padilha, A.L., Vitorello, Í., Pádua, M.B., 2013. Anomalous electrical structure in the northwestern Paraná Basin, Brazil, observed with broadband magnetotellurics. *J. S. Am. Earth Sci.* <https://doi.org/10.1016/j.jsames.2012.07.006>.
- Bologna, M.S., Padilha, A.L., Pádua, M.B., Vitorello, Í., Chamalaun, F.H., 2014. Paraguay-Araguaia belt conductivity anomaly: a fundamental tectonic boundary in South American platform imaged by electromagnetic induction surveys. *Geochem. Geophys. Geosyst.* 15, 509–515. <https://doi.org/10.1002/2013GC004970>.
- Bologna, M.S., Egbert, G.D., Padilha, A.L., Pádua, M.B., Vitorello, Í., 2017. 3-D inversion of complex magnetotelluric data from an Archean-Proterozoic terrain in northeastern São Francisco Craton, Brazil. *Geophys. J. Int.* 210, 1545–1559. <https://doi.org/10.1093/gji/ggx261>.
- Bologna, M.S., Dragone, G.N., Muzio, R., Peel, E., Nuñez-Demarcó, P., Ussami, N., 2019. Electrical structure of the lithosphere from Rio de la Plata Craton to Paraná Basin: amalgamation of cratonic and reformed lithospheres in SW Gondwanaland. *Tectonics* 38, 77–94. <https://doi.org/10.1029/2018TC005148>.
- Caldwell, T.G., Bibby, H.M., Brown, C., 2004. The magnetotelluric phase tensor. *Geophys. J. Int.* 158, 457–469. <https://doi.org/10.1111/j.1365-246X.2004.02281.x>.
- Chaves, C., Ussami, N., Ritsama, J., 2016. Density and P-wave velocity structure beneath the Paraná Magmatic Province: Refertilization of an ancient lithospheric mantle. *Geochem. Geophys. Geosyst.* <https://doi.org/10.1002/2016GC006369>.
- Chaves, C.A.M., Ussami, N., 2013. Modeling 3-D density distribution in the mantle from inversion of geoid anomalies: application to the Yellowstone Province. *J. Geophys. Res.* 118 (12), 6328–6351. <https://doi.org/10.1002/2013JB010168>.
- Comin-Chiaromonte, P., Lucassen, F., Girardi, V.A.V., De Min, A., Gomes, C.B., 2010. Lavas and their mantle xenoliths from intracratonic Eastern Paraguay (South America Platform) and Andean Domain, NW-Argentina: a comparative review. *Mineral. Petrol.* 98, 143–165. <https://doi.org/10.1007/s00710-009-0061-6>.
- Corbo, F., Arzate, J., Oleaga, A., 2012. Structure of the Guaraní aquifer in the surroundings of the Uruguay river from magnetotelluric soundings. *Geofis. Int.* 51, 17–37.
- Cordani, U.G., Cubas, N., Sato, K., Nutman, A.P., Gonzales, M.E., Pressner, J.L.B., 2001. Geochronological Constraints for the Evolution of the Metamorphic Complex near the Tebicuary River, Southern Precambrian Region of Paraguay. Paper presented at III Simposio Sudamericano de Geología Isotópica, Pucon, Chile.
- Dragone, G.N., Ussami, N., Gimenez, M.E., Lince Klingler, F.G., Chaves, C.A.M., 2017. Western Paraná suture/shear zone and the limits of Rio Apa, Rio Tebicuary and Rio de la Plata cratons from gravity data. *Precambrian Res.* 291 <https://doi.org/10.1016/j.precamres.2017.01.029>.
- Egbert, G.D., 1997. Robust multiple-station magnetotelluric data processing. *Geophys. J. Int.* 130, 475–496. <https://doi.org/10.1111/j.1365-246X.1997.tb05663.x>.
- Evans, R.L., 2012. Chapter 3: Earths electromagnetic environment. Part 1: Conductivity of earth materials. In: Chave, A.D., Jones, A.G. (Eds.), *The Magnetotelluric Method: Theory and Practice*. Cambridge Univ. Press, New York, pp. 50–95.
- Evans, R.L., Jones, A.G., Garcia, X., Muller, M., Hamilton, M., Evans, S., Fourie, C.J.S., Spratt, J., Webb, S., Jelsma, H., Hutchins, D., 2011. Electrical lithosphere beneath the Kaapvaal craton, southern Africa. *J. Geophys. Res.* 116, B04105 <https://doi.org/10.1029/2010JB007883>.
- Favetto, A., Pomposiello, C., López de Luchi, M.G., Booker, J., 2008. 2D Magnetotelluric interpretation of the crust electrical resistivity across the Pampean terrane–Rio de la Plata suture, in Central Argentina. *Tectonophysics* 459, 54–65. <https://doi.org/10.1016/j.tecto.2007.11.071>.
- Favetto, A., Rocha, V., Pomposiello, C., García, R., Barcelona, H., 2015. A new limit for the NW Río de la Plata Craton Border at about 24oS (Argentina) detected by Magnetotellurics. *Geol. Acta* 13, 243–254.
- Frugis, G.L., da Costa Campos Neto, Mario, Lima, R.B., 2018. Eastern Paranapanema and southern São Francisco orogenic margins: Records of enduring Neoproterozoic oceanic convergence and collision in the southern Brasília Orogen. *Precambrian Res.* <https://doi.org/10.1016/j.precamres.2018.02.005>.
- Fyfe, W.S., 1978. The evolution of the Earth's crust: modern plate tectonics to ancient hot spot tectonics? *Chem. Geol.* 23, 89–114. [https://doi.org/10.1016/0009-2541\(78\)90068-2](https://doi.org/10.1016/0009-2541(78)90068-2).
- Griffin, W.L., O'Reilly, S.Y., Afonso, J.C., Begg, G.C., 2009. The composition and evolution of lithospheric mantle: a re-evaluation and its tectonic implications. *J. Petrol.* 50 (7), 1185–1204. <https://doi.org/10.1093/ptrology/egn033>.
- Ingham, M.R., 1988. The use of invariant impedances in magnetotelluric interpretation. *Geophys. J. Int.* 92 (1), 165–169. <https://doi.org/10.1111/j.1365-246X.1988.tb01130.x>.
- Jones, A.G., Ledo, J., Ferguson, I.J., 2005. Electromagnetic images of the Trans-Hudson orogen: the north American Central Plains anomaly revealed. *Can. J. Earth Sci.* <https://doi.org/10.1139/e05-018>.
- Kelbert, A., Meqbel, N., Egbert, G.D., Tandon, K., 2014. ModEM: a modular system for inversion of electromagnetic geophysical data. *Comput. Geosci.* 66, 40–53. <https://doi.org/10.1016/j.cageo.2014.01.010>.
- Khoza, T.D., Jones, A.G., Muller, M.R., Evans, R.L., Miensopust, M.P., Webb, S.J., 2013. Lithospheric structure of an Archean craton and adjacent mobile belt revealed from 2-D and 3-D inversion of magnetotelluric data: example from southern Congo craton in northern Namibia. *J. Geophys. Res. Solid Earth* 118, 4378–4397. <https://doi.org/10.1002/jgrb.50258>.
- Lee, C.-T.A., 2003. Compositional variation of density and seismic velocities in natural peridotites at STP conditions: implications for seismic imaging of compositional heterogeneities in the upper mantle. *J. Geophys. Res.* 108 (B9), 2441. <https://doi.org/10.1029/2003jb002413>.
- Leite, A.F.G.D., de Sousa, M.Z.A., Ruiz, A.S., Cubas, N., de Matos, J.B., Dantas, E.L., de Oliveira, J.R., 2018. Petrology and geochronology (U Pb) of the Caapucú suite – Southern Paraguay: POST-TECTONIC magmatism of the Paraguari belt. *J. S. Am. Earth Sci.* 88, 621–641. <https://doi.org/10.1016/j.jsames.2018.09.016>.
- Lohse, B., 1990. *Petrographische und geochronologische Erkenntnisse über den Westteil des Tebicuary-Kratons*. In: Südost Paraguay (Doctoral Dissertation). Heidelberg University, Heidelberg, Germany.
- Mariani, P., Braitenberg, C., Ussami, N., 2013. Explaining the thick crust in Paraná basin, Brazil, with satellite GOCE gravity observations. *J. S. Am. Earth Sci.* 45, 209–223. <https://doi.org/10.1016/j.jsames.2013.03.008>.
- Marques, L.S., Dupré, B., Piccirillo, E.M., 1999. Mantle source compositions of the Paraná Magmatic Province (southern Brazil): evidence from trace element and Sr-Nd-Pb isotope geochemistry. *J. Geodyn.* [https://doi.org/10.1016/S0264-3707\(99\)00020-4](https://doi.org/10.1016/S0264-3707(99)00020-4).
- Maurya, V.P., Meju, M.A., Fontes, S.L., Padilha, A.L., La Terra, E.F., Miquelutti, L.G., 2018. Deep resistivity structure of basalt-covered central part of Paraná Basin, Brazil, from joint 3-D MT and GDS data imaging. *Geochem. Geophys. Geosyst.* 19, 1994–2013. <https://doi.org/10.1029/2017GC007314>.
- Maus, S., 2010. An ellipsoidal harmonic representation of Earth's lithospheric magnetic field to degree and order 720. *Geochem. Geophys. Geosyst.* 11 <https://doi.org/10.1029/2010GC003026>.
- Meqbel, N., Weckmann, U., Muñoz, G., Ritter, O., 2016. Crustal metamorphic fluid flux beneath the Dead Sea Basin: constraints from 2-D and 3-D magnetotelluric modelling. *Geophys. J. Int.* 207, 1609–1629. <https://doi.org/10.1093/gji/ggw359>.

- Meqbel, N.M., Egbert, G.D., Wannamaker, P.E., Kelbert, A., Schultz, A., 2014. Deep electrical resistivity structure of the northwestern U.S. derived from 3-D inversion of USArray magnetotelluric data. *Earth Planet. Sci. Lett.* <https://doi.org/10.1016/j.epsl.2013.12.026>.
- Milani, E.J., Ramos, V.A., 1998. Orogenias Paleozóicas no Domínio Sul-Occidental do Gondwana e os Ciclos de Subsidência da Bacia do Paraná. *Rev. Bras. Geociências* 28, 473–484. <https://doi.org/10.25249/0375-7536.1998473484>.
- Milani, E.J., Zalán, P.V., 1999. An outline of the geology and petroleum systems of the Paleozoic interior basins of South America. *Episodes* 22, 199–205. <https://doi.org/10.18814/epiugs/1999/v22i3/007>.
- Olsen, N., 1999. Long-period (30 days-1 year) electromagnetic sounding and the electrical conductivity of the lower mantle beneath Europe. *Geophys. J. Int.* <https://doi.org/10.1046/j.1365-246X.1999.00854.x>.
- Oriolo, S., Oyhantcábal, P., Wemmer, K., Basei, M.A.S., Benowitz, J., Pfänder, J., Hannich, F., Siegesmund, S., 2016. Timing of deformation in the Sarandí del Yí Shear Zone, Uruguay: Implications for the amalgamation of western Gondwana during the Neoproterozoic Brasiliano-Pan-African Orogeny. *Tectonics* 35, 754–771. <https://doi.org/10.1002/2015TC004052>.
- Orozco, L.A., Favetto, A., Pomposiello, C., Rossello, E., Booker, J., 2013. Crustal deformation of the Andean foreland at 31° 30'S (Argentina) constrained by magnetotelluric survey. *Tectonophysics* 582, 126–139. <https://doi.org/10.1016/j.tecto.2012.09.030>.
- Oyhantcábal, P., Siegesmund, S., Wemmer, K., 2011. The Río de la Plata Craton: a review of units, boundaries, ages and isotopic signature. *Int. J. Earth Sci.* 100, 201–220. <https://doi.org/10.1007/s00531-010-0580-8>.
- Padilha, A.L., Vitorello, I., Pádua, M.B., 2013. Deep conductivity structure beneath the northern Brasília belt, Central Brazil: evidence for a Neoproterozoic arc-continent collision. *Gondwana Res.* 23, 748–758. <https://doi.org/10.1016/j.gr.2012.05.016>.
- Padilha, A.L., Vitorello, I., Antunes, C.E., Pádua, M.B., 2015. Imaging three-dimensional crustal conductivity structures reflecting continental flood basalt effects hidden beneath thick intracratonic sedimentary basin. *J. Geophys. Res. Solid Earth* 120, 4702–4719. <https://doi.org/10.1002/2014JB011657>.
- Patro, P.K., Uyeshima, M., Siripunvaraporn, W., 2013. Three-dimensional inversion of magnetotelluric phase tensor data. *Geophys. J. Int.* 192, 58–66. <https://doi.org/10.1093/gji/ggs014>.
- Peate, D.W., Hawkesworth, C.J., Mantovani, M.S.M., 1992. Chemical stratigraphy of the Paraná lavas (South America): classification of magma types and their spatial distribution. *Bull. Volcanol.* <https://doi.org/10.1007/BF00301125>.
- Peri, V.G., Pomposiello, M.C., Favetto, A., Barcelona, H., Rossello, E.A., 2013. Magnetotelluric evidence of the tectonic boundary between the Río de la Plata Craton and the Pampean terrane (Chaco-Pampean Plain, Argentina): the extension of the Transbrasiliano Lineament. *Tectonophysics* 608, 685–699. <https://doi.org/10.1016/j.tecto.2013.08.012>.
- Peri, V.G., Barcelona, H., Pomposiello, M.C., Favetto, A., 2015. Magnetotelluric characterization through the Ambargasta-Sumampa Range: the connection between the northern and southern trace of the Río de la Plata Craton – Pampean Terrane tectonic boundary. *J. S. Am. Earth Sci.* 59, 1–12. <https://doi.org/10.1016/j.jsames.2015.01.003>.
- Pezzi, E.E., Moztetic, M.E., 1989. Cuencas Sedimentarias de la Región Chacoparanense. In: Chebli, G.A., Spalletti, L. (Eds.), *Cuencas Sedimentarias Argentinas, Serie Correlación Geológica, n. 6*. Universidad Nacional de Tucumán, Tucumán, Argentina, pp. 65–78.
- Piccirillo, E.M., Civetta, L., Petrini, R., Longinelli, A., Bellieni, G., Comin-Chiaromonte, P., Marques, L.S., Melfi, A.J., 1989. Regional variations within the Paraná flood basalts (southern Brazil): evidence for subcontinental mantle heterogeneity and crustal contamination. *Chem. Geol.* [https://doi.org/10.1016/0009-2541\(89\)90023-5](https://doi.org/10.1016/0009-2541(89)90023-5).
- Pimentel, M.M., Fuck, R.A., 1992. Neoproterozoic crustal accretion in central Brazil. *Geology* 20, 375–379. [https://doi.org/10.1130/0091-7613\(1992\)020<0375:NCAICB>2.3.CO;2](https://doi.org/10.1130/0091-7613(1992)020<0375:NCAICB>2.3.CO;2).
- Pimentel, M.M., Fuck, R.A., Jost, H., Ferreira Filho, C.F., Araújo, S.M., 2000. The basement of the Brasília fold belt and the Goiás magmatic arc. In: Cordani, U.G., Milani, E.J., Filho, A. Thomaz, Campos, D.A. (Eds.), *Tectonic Evolution of South America. 31st International Geological Congress, Rio de Janeiro, Brazil*, pp. 195–229.
- Poudjom-Djomani, Y.H., O'Reilly, S.Y., Griffin, W.L., Morgan, P., 2001. The density structure of SL through time. *Earth Planet. Sci. Lett.* 184, 605–621. [https://doi.org/10.1016/S0012-821X\(00\)00362-9](https://doi.org/10.1016/S0012-821X(00)00362-9).
- Ramos, V.A., 1988. Late Proterozoic-early Paleozoic of South America - a collisional history. *Episodes* 11, 168–174. <https://doi.org/10.18814/epiugs/1988/v11i3/003>.
- Rapela, C.W., Pankhurst, R.J., Casquet, C., Fanning, C.M., Baldo, E.G., González-Casado, J.M., Galindo, C., Dahlquist, J., 2007. The Río de la Plata craton and the assembly of SW Gondwana. *Earth Sci. Rev.* 83, 49–82. <https://doi.org/10.1016/j.earscirev.2007.03.004>.
- Rapela, C.W., Fanning, C.M., Casquet, C., Pankhurst, R.J., Spalletti, L., Poiré, D., Baldo, E.G., 2011. The Río de la Plata craton and the adjoining Pan-African/Brasiliano terranes: their origins and incorporation into south-West Gondwana. *Gondwana Res.* 20, 673–690. <https://doi.org/10.1016/j.gr.2011.05.001>.
- Renne, P.R., Ernesto, M., Pacca, I.G., Coe, R.S., Glen, J.M., Prévot, M., Perrin, M., 1992. The age of Paraná flood volcanism, rifting of Gondwanaland, and the Jurassic-cretaceous boundary. *Science* 258 (5084), 975–979. <https://doi.org/10.1126/science.258.5084.975>.
- Rivadeneira-Vera, C., Bianchi, M., Assumpção, M., Cedraz, V., Juliá, J., Rodríguez, M., Sánchez, L., Sánchez, G., Lopez-Murua, L., Fernandez, G., Fugarazzo, R., 2019. An Updated Crustal Thickness Map of Central South America based on Receiver Function Measurements in the Region of the Chaco, Pantanal, and Paraná Basins, Southwestern Brazil. *J. Geophys. Res. Solid Earth* 124, 8491–8505. <https://doi.org/10.1029/2018JB016811>.
- Rocha, M.P., Assumpção, M., Affonso, G.M.P.C., Azevedo, P.A., Bianchi, M., 2019. Teleseismic P Wave Tomography beneath the Pantanal, Paraná, and Chaco-Paraná Basins, SE South America: Delimiting Lithospheric Blocks of the SW Gondwana Assemblage. *J. Geophys. Res. Solid Earth.* <https://doi.org/10.1029/2018JB016807>.
- Rocha-Júnior, E.R.V., Marques, L.S., Babinski, M., Nardy, A.J.R., Figueiredo, A.M.G., Machado, F.B., 2013. Sr-Nd-Pb isotopic constraints on the nature of the mantle sources involved in the genesis of the high-Ti tholeiites from northern Paraná Continental Flood Basalts (Brazil). *J. S. Am. Earth Sci.* <https://doi.org/10.1016/j.jsames.2013.04.004>.
- Rocha-Júnior, E.R.V., Marques, L.S., Babinski, M., Machado, F.B., Petronilho, L.A., Nardy, A.J.R., 2020. A telltale signature of Archean lithospheric mantle in the Paraná continental flood basalts genesis. *Lithos* 364–365 (105519). <https://doi.org/10.1016/j.lithos.2020.105519>.
- de Sá, N.C., 2004. O campo de gravidade, o geóide e a estrutura crustal na América do Sul: novas estratégias de representação (Habilitation thesis). Universidade de São Paulo, São Paulo, Brazil.
- Schenk, C.J., Viger, R.J., Anderson, C.P., 1999. Maps Showing Geology, Oil and Gas Fields and Geologic Provinces of the South America Region: U.S. Geological Survey Open-File Report 97–470-D (12 p). <https://doi.org/10.3133/ofr97470D> (last access on 27/07/2020).
- Selway, K., 2014. On the causes of electrical conductivity anomalies in tectonically stable lithosphere. *Surv. Geophys.* 35, 219–257. <https://doi.org/10.1007/s10712-013-9235-1>.
- Shirzad, T., Assumpcao, M., Bianchi, M., 2020. Ambient seismic noise tomography in west-central and Southern Brazil, characterizing the crustal structure of the Chaco-Paraná, Pantanal and Paraná basins. *Geophys. J. Int.* <https://doi.org/10.1093/gji/ggz548>.
- Smith, W.H.F., Wessel, P., 1990. Gridding with continuous curvature splines in tension. *Geophysics* 55, 293–305. <https://doi.org/10.1190/1.1442837>.
- Tarits, P., Hautot, S., Perrier, F., 2004. Water in the mantle: results from electrical conductivity beneath the French Alps. *Geophys. Res. Lett.* <https://doi.org/10.1029/2003gl019277>.
- Thiede, D.S., Vasconcelos, P.M., 2010. Paraná flood basalts: rapid extrusion hypothesis confirmed by new 40Ar/39Ar results. *Geology* 38, 747–750. <https://doi.org/10.1130/G30919.1>.
- Tietze, K., Ritter, O., 2013. Three-dimensional magnetotelluric inversion in practice—the electrical conductivity structure of the San Andreas Fault in Central California. *Geophys. J. Int.* 195, 130–147. <https://doi.org/10.1093/gji/ggt234>.
- Tohver, E., Cawood, P.A., Rossello, E.A., Jourdan, F., 2012. Closure of the Clymene Ocean and formation of West Gondwana in the Cambrian: evidence from the Sierras Australes of the southernmost Río de la Plata craton, Argentina. *Gondwana Res.* 21, 394–405. <https://doi.org/10.1016/j.gr.2011.04.001>.
- Trindade, R.I.F., D'Agrella-Filho, M.S., Epof, I., Brito Neves, B.B., 2006. Paleomagnetism of early Cambrian Itabaiana mafic dikes (NE Brazil) and the final assembly of Gondwana. *Earth Planet. Sci. Lett.* <https://doi.org/10.1016/j.epsl.2005.12.039>.
- Wessel, P., Smith, W.H.F., 1991. Free software helps map and display data. *Eos Trans. AGU* 72 (41), 441–446. <https://doi.org/10.1029/90EO00319>.
- Wessel, P., Smith, W.H.F., Scharroo, R., Luis, J.F., Wobbe, F., 2013. Generic mapping tools: improved version released. *Eos Trans. AGU* 94, 409–410 (2013). <https://doi.org/10.1002/2013EO450001>.
- Xu, Y., Shankland, T.J., Duba, A.G., 2000a. Pressure effect on electrical conductivity of mantle olivine. *Phys. Earth Planet. Inter.* [https://doi.org/10.1016/S0031-9201\(99\)00135-1](https://doi.org/10.1016/S0031-9201(99)00135-1).
- Xu, Y., Shankland, T.J., Poe, B.T., 2000b. Laboratory-based electrical conductivity in the Earth's mantle. *J. Geophys. Res. Solid Earth.* <https://doi.org/10.1029/2000jb900299>.
- Yang, B., Egbert, G.D., Kelbert, A., Meqbel, N.M., 2015. Three-dimensional electrical resistivity of the north-Central USA from EarthScope long period magnetotelluric data. *Earth Planet. Sci. Lett.* <https://doi.org/10.1016/j.epsl.2015.04.006>.